How Peptides Dissociate in Plasmonic Hot Spots

Journal Article

Author(s):
Szczerbiński, Jacek; Metternich, Jonas B.; Goubert, Guillaume (iD); Zenobi, Renato (iD)

1 # How peptides dissociate in plasmonic hot spots

2 Jacek Szczerbiński, Jonas B. Metternich, Guillaume Goubert and Renato Zenobi*

3 Department of Chemistry and Applied Biosciences, Laboratory of Organic Chemistry,
4 ETH Zurich, 8093 Zurich, Switzerland, e–mail: zenobi@org.chem.ethz.ch

5 Abstract

6 Plasmon–induced hot carriers enable dissociation of strong chemical bonds by visible
7 light. This unusual chemistry has been demonstrated for several diatomic and small
8 organic molecules. Here we extend the scope of plasmon–driven photochemistry to
9 biomolecules and describe the reactivity of proteins and peptides in plasmonic hot spots.
10 We use tip–enhanced Raman spectroscopy (TERS) to both drive the reactions and to
11 monitor their products. Peptide backbone bonds are found to dissociate in the hot spot,
12 which is reflected in the disappearance of the amide I band in the TER spectra. The
13 observed fragmentation pathway involves non–thermal activation, presumably by
14 dissociative capture of a plasmon–induced hot electron. This fragmentation pathway is
15 known from electron transfer dissociation (ETD) of peptides in gas–phase mass
16 spectrometry (MS), which suggests a general similarity between plasmon–induced
17 photochemistry and nonergodic reactions triggered by electron capture. This analogy
18 may serve as a design principle for plasmon–induced reactions of biomolecules.

19 **Keywords:** hot electrons, plasmon–driven photocatalysis, tip–enhanced Raman
20 spectroscopy, electron transfer dissociation, peptides, amide I band

21
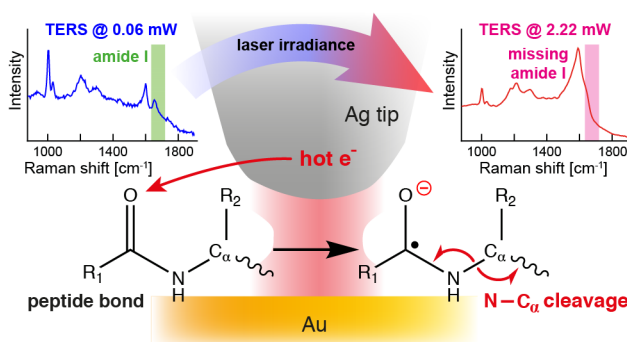
Introduction

Plasmon–induced hot carriers have attracted the attention of catalysis research, because they can be utilized to accelerate reactions with visible light[1–3]. They also enable the formation of unusual reaction products via non–thermal activation of the reactants[4,5]. Since the field is new, the scope of chemistry that can be driven by hot carriers has not yet been fully explored and so far includes mostly small molecules (like H_2, O_2 and NH_3)[2,3,6] and model organic molecules (mostly thiols, biphenyls and bipyridines)[4,7–10]. Recently it was proposed[5,11] that plasmon–induced reactions rely on the same mechanism as desorption induced by electronic transitions (DIET)[11–14] – a process well known from surface science studies of small molecules adsorbed on planar metal surfaces (electron stimulated desorption[15], surface femtochemistry[16,17], x–ray photochemistry[18] *etc*.). DIET relies on the transfer of a hot electron from the metal to an adsorbed molecule, which triggers nonergodic bond dissociation, *i. e.* occurring faster than a molecular vibration (below 10^{-14} s)[13]. The chemical transformation takes place before the molecule reaches thermal equilibrium via exchange of energy between its internal degrees of freedom. Hence, the reactivity of the radical formed upon electron capture may be very different from that of the neutral precursor. Consequently, DIET results in non–thermal fragmentation pathways that may not involve the weakest bond of the neutral adsorbate, but the one that is destabilized through the attachment of a low–energy electron. The similarity between plasmon–assisted photochemistry and DIET is helpful in understanding and developing novel plasmon–assisted reactions, however it has been restricted to small molecules investigated by surface science in high vacuum conditions.

Over the last decade several groups have demonstrated that plasmon–induced reactions can occur during measurements with surface– and tip–enhanced Raman spectroscopy

46 (SERS and TERS)[4,5,9,19]. These reactions are perceived detrimental for plasmon–

47 enhanced spectroscopies, because they change the investigated sample during the

48 measurement[5,19]. This has become a pressing issue in the last decade, when TERS was

49 applied for nanoscale spectroscopic imaging of native protein assemblies[20],[21] (Fig. 1A).

50 The photochemical degradation of the analyte leads to missing spectral features, large

51 fluctuations in the spectra[5,22–24] and lack of resemblance to the bulk Raman spectra of

52 the same molecules[25–33]. In particular, the amide I band (which is the clearest Raman

53 marker of peptide bonds) is frequently missing in the SER/TER spectra of proteins and

54 peptides[34,35] (Fig. 1B, see detailed discussion in Section S1 of the Supporting

55 Information). This has been a long–lasting controversy in the SERS/TERS community,

56 with dedicated studies published on the topic by Blum *et al.*[34] and Kurouski *et al.*[35] The

57 proposed explanations of the absence of the amide I band included (among others)

58 shielding of the amide bond by bulky amino acid residues, chemical interaction between

59 Au and the peptide backbone, as well as differences in the selection rules between tip–

60 enhanced and normal Raman spectroscopy[34–36].
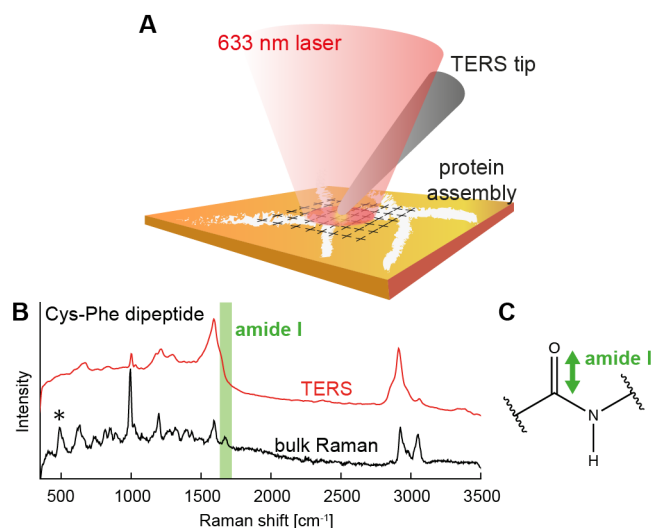
Figure 1. (A) TERS imaging of a protein assembly: the TERS tip is raster–scanned over a sample deposited on a flat surface, and a TER spectrum is acquired at every pixel of the raster, yielding a nanoscale chemical image of the sample. In the case of protein imaging, the local conformation of the protein residing under the tip can, in principle, be mapped based on the positions of the amide bands in the TER spectrum. (B) Bulk Raman and TER spectra of a dipeptide Cys–Phe. The amide I band (1630–1680 cm^{-1}) is a Raman marker of peptide bonds, which, however, is frequently missing in published SER/TER spectra of peptides and proteins. The ν(S–S) vibration of Cys–Phe at 500 cm^{-1} (marked with an asterisk *) in the bulk Raman spectrum is also absent in the TER spectrum, but for a different reason – cleavage of the disulfide bonds upon binding of the peptide to the Au surface through formation of Au–S bonds. (C) The amide I vibrational mode consists mostly of the C=O stretching vibration in the peptide bond, with contributions from the C–N stretch and the C–C–N deformation.

The discrepancy between bulk Raman and TER spectra of peptides is problematic and raises questions regarding the reliability of peak assignments in TERS. In order to address these issues, SERS researchers have developed means to improve the reproducibility of the spectra of proteins, including pre–cleaning the surface of the SERS substrates[37,38], reducing the interaction time between the protein and the nanostructure[39], and coating the Ag nanoparticles with protective chemical layers[40–42]. These approaches result in

4

79   clean spectra of proteins, including data where the amide I band is visible, but similarly

80   clean data sets have not been reported in the TERS literature.

81   Here, we employ TERS to study the reactivity of peptides and proteins in plasmonic hot

82   spots. Contrary to DIET experiments, TERS can be performed in ambient conditions, and

83   thus can accommodate a much broader scope of reactants, including biomolecules.

84   Comparison of TERS with MS/MS fragmentation techniques reveals nonergodic

85   dissociation of proteins and peptides in plasmonic hot spots, which allows us to propose

86   a general description of the underlying plasmon–driven chemistry. Furthermore, we

87   explain the impact of the plasmon–induced reactions on the TER spectra of biomolecules

88   and provide experimental guidelines to avoid sample degradation and maintain

89   consistency with bulk Raman spectra.

90   **Results**

91   In order to understand the reactivity of peptides in plasmonic hot spots, we performed

92   TERS measurements on 10 model compounds containing amide bonds (Fig. 2): two small

93   synthetic amides (<0.2 kDa), five di– and tri–peptides (0.25–0.50 kDa), two oligopeptides

94   composed of 16–20 amino acids (~2 kDa), and a protein with a molecular weight of 66

95   kDa. Thin molecular layers of the samples were prepared on a flat Au surface via self–

96   assembly, spin coating or dried droplet deposition (see Methods). TER spectra were

97   acquired at points on a grid cast over a square region on the sample, like in TERS imaging

98   (Fig. 1A). The large number of systems investigated in this study and the wide range of

99   their sizes enable general conclusions to be drawn on plasmon–induced photochemistry

100 of peptides and proteins. Below, we first describe the disappearance of the amide I band

101 from the TER spectra of peptides, and then we explain the underlying chemistry.
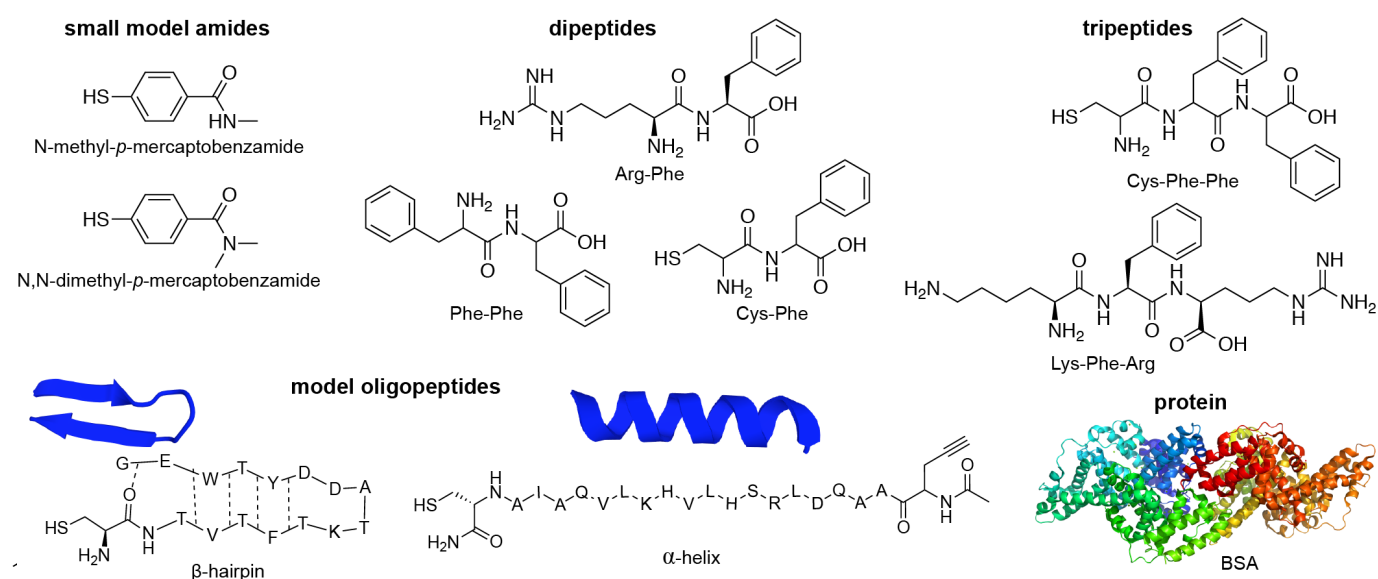
104 **Is the amide I band visible in TERS?** Photochemical transformations in plasmonic hot

105 spots rely primarily on dissociative attachment of plasmon–induced hot electrons to the

106 molecules under the tip[5,11]. These charge–driven reactions act in synergy with thermal

107 excitation[3,5,11], because electronic transitions are easier to initiate from a vibrationally

108 excited state. Therefore, we performed TERS measurements tuning both the laser power

109 (0.007 – 2.840 mW) and the temperature in the hot spot. The temperature under the TERS

110 tip depends not only on the laser power applied, but also on the size of the TERS image:

111 the smaller the scan area, the more heat accumulates under the tip, resulting in higher

112 temperature (for further discussion see Section S2). Hence, the temperature in the hot

113 spot was controlled partially independent of the laser irradiance, by varying the size of

114 the scan size ($0.13 \times 0.13 - 1 \times 1$ μm² squares, see Fig. 3A).

115 Fig. 3 illustrates the disappearance of the amide I band for three peptides of different

116 sizes: a dipeptide Arg–Phe (Fig. 3B), a β–hairpin oligopeptide with 16 amino acids (Fig.

117 3C), and the protein bovine serum albumin (BSA, Fig. 3D). Both β–hairpin and BSA were

118 terminated with Cys residues to facilitate the formation of a monolayer on the Au surface.

119   The spectra depicted in blue in Fig. 3B,C,D were acquired at low laser exposure and

120   resemble the bulk Raman spectra (black traces) of the same peptides, including the

121   presence of the amide I band (highlighted in green). Small discrepancies are likely due to

122   the binding of the peptide to Au through nitrogen, sulfur (see Fig. 1B), or π–π adsorption

123   of the phenyl ring. Upon increasing the laser exposure (higher power, smaller scan size),

124   the amide I band gradually disappears, and other symptoms of sample degradation arise

125   as well.
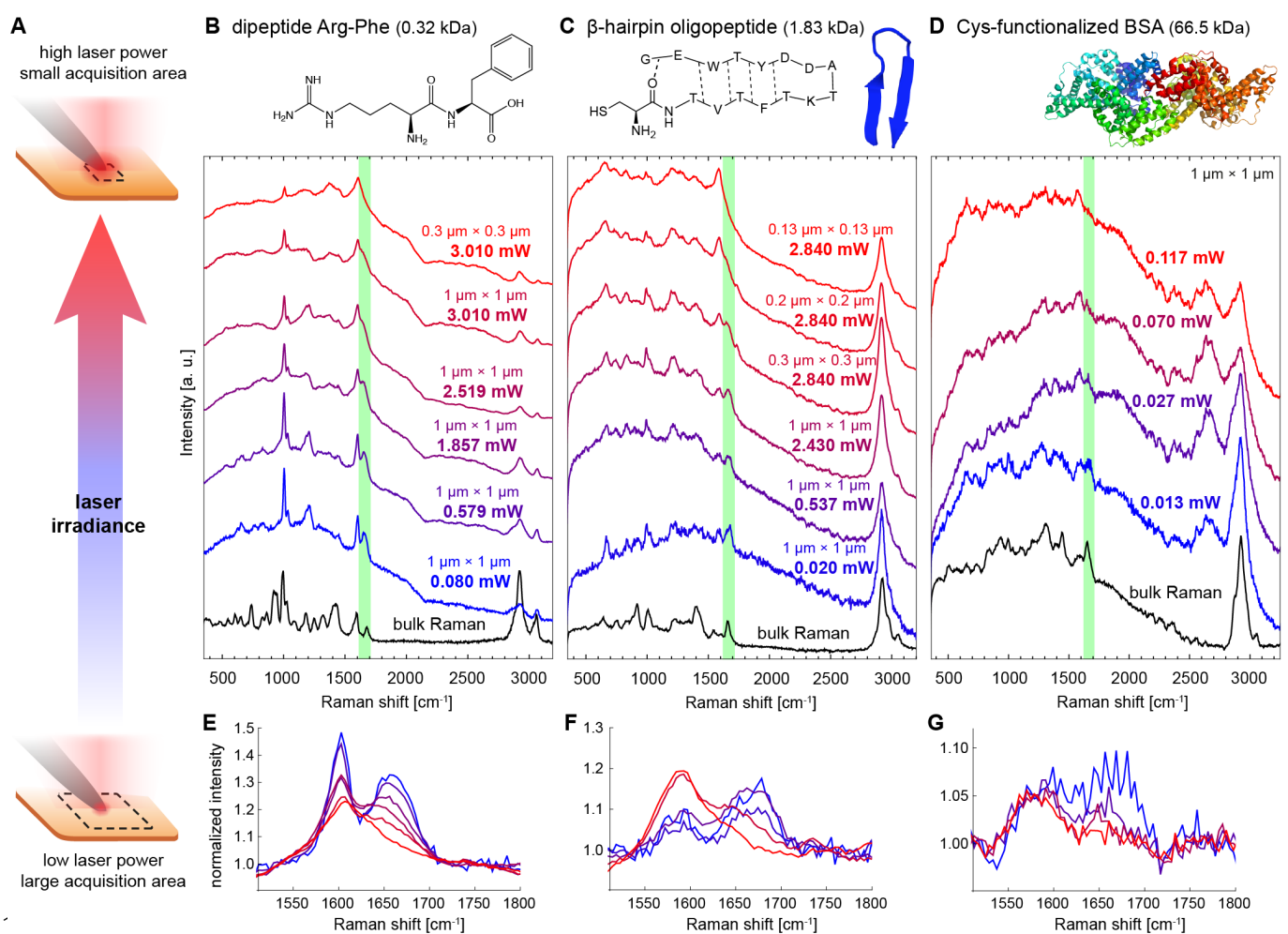
127   **Figure 3.** Plasmon–induced backbone cleavage in peptides of various sizes. (A) TER spectra were acquired

128   in imaging mode, similar to Fig. 1A. The laser power and scan size affect the rate of photoinduced sample

129   degradation in (B) a dipeptide Arg–Phe, (C) a β–hairpin oligopeptide, (D) a Cys–terminated BSA. The amide

130   I mode (highlighted in green) is visible in the TER spectra acquired at low laser exposure (blue traces).

131   These TER spectra are in reasonable agreement with the bulk Raman spectra of the same molecules (black

132   traces). The amide I band disappears upon increasing the laser irradiance, due to plasmon–induced

133   dissociation of the peptide backbone. The spectra are scaled to fit together in one graph, but not

134   background–corrected. (E, F, G) Zoom into the amide I region of the TER spectra. The background was

135   corrected by dividing of the spectra by the linear baseline fit.

136   Figures S2–S5 show a similar behavior for three other di– and tripeptides and an α–helical

137   oligopeptide with 20 amino acids. In all cases, the amide I band is clearly visible in the

138   spectra acquired at low laser exposure, regardless of the size and the amino acid

139   composition of the peptide. Consequently, the disappearance of the amide I band from the

140   TER spectra of peptides is an artifact, caused by inadequate measurement conditions.

141   More specifically, acquisition of TER spectra results in degradation of the analyte at high

142   laser irradiance and prolonged residence of the tip on a small region of the sample. As

143   shown in our recent work for model thiols[5], the tip–induced sample degradation is

144   primarily a function of the incident laser irradiance, whereas the irradiation time is of

145   secondary importance.

146   Our findings contradict the hypothesis of steric shielding of the amide bond by bulky

147   amino acid residues proposed by Chumanov *et al.*[36] and Kurouski *et al.*[35]. Yet, similar to

148   these authors, we always observe the bands corresponding to the amino acid residues,

149   even if the amide I band is absent (*cf.* hexa–Tyr peptide in ref. [35]). We explain this

150   observation by preferential dissociation of the peptide backbone upon attachment of a

151   hot electron, resulting in disappearance of amide I, but not affecting the signal from the

152   side chains. For some amino acids the dissociative electron capture proceeds further and

153   affects the residues at higher laser irradiance – for example, guanidine can be released

154   from the Arg residues in argininamide (Fig. S5) and Lys–Phe–Arg (see below). However,

155   for most amino acids, the dissociation of the residue requires higher energy of the hot

156 electron than the backbone cleavage, so the disappearance of the amide I band is observed

157 first.

158 Surprisingly, the exact position of the amide I band in the TER spectra does not always

159 match the position of its bulk Raman counterpart. This is discussed in detail in the

160 Supporting Information (Section S3).

161 **How does the peptide backbone cleave?** As outlined in the introduction, plasmon–

162 driven reactions are analogous to DIET, a class of electron attachment reactions known

163 from surface science[5,11]. We hypothesize that photochemical transformations in

164 plasmonic hot spots are also analogous to gas–phase reactions, where a 1–2 eV electron

165 attaches to the molecule and triggers its dissociation. Below we demonstrate that

166 dissociation of peptides under the TERS tip leads to products similar to those observed in

167 electron capture dissociation and ETD of peptides in the gas phase.

168 In ETD MS, a peptide M under study is gently ionized by electrospray ionization to obtain

169 intact, protonated peptide ions with various charge states $[M + nH]^{n+}$. The desired charge

170 state is mass–selected by removal of all other ions, including fragments formed during

171 ionization and desolvation. The isolated peptide ions are stored in an ion trap and

172 undergo collisions with a negatively charged electron transfer reagent, which donates a

173 low energy (1–2 eV) electron to the peptide. Upon attachment of the electron, the

174 $[M + nH]^{n+}$ cation is reduced to a reactive $[M + nH]^{(n-1)+\bullet}$ radical, which is prone to

175 dissociation via cleavage of the peptide backbone, or of the amino acid residues.

176 Importantly, the capture of a single electron results in a cascade of radical reactions,

177 leading to several backbone cleavages and side chain losses within the same peptide[43].

178 ETD is frequently employed in MS/MS analysis of proteins, because it allows

179   fragmentation of macromolecules into smaller peptides, which enables sequencing and

180   analysis of post–translational modifications[44].

181   Similar to DIET reactions[13], ETD is a nonergodic process resulting in non–thermal

182   fragmentation pathways[45]. The fragmentation rules are very characteristic to ETD and

183   different from fragmentation techniques that rely on thermal activation of the ion, for

184   example collision–induced dissociation (CID). Typical fragmentation pathways of the

185   peptide backbone in ETD and CID are shown in Fig. 4 A and B, respectively. In ETD of

186   peptides, the low energy electron attaches to the amide π^* system, forming an enol–

187   imidate radical anion[46]. The radical cleaves the $N–C_\alpha$ bond, and the anion is neutralized

188   by proton transfer from a charged or neutral site in the vicinity (typically the residue of a

189   neighbor Arg or Lys). The dissociation leads to the formation of a *c* type fragment, which

190   is a primary amide or the enolimine tautomer (less favored), and of a *z* type fragment,

191   which consists of the C–terminal end of the peptide chain without the N–terminus.

192   In contrast, CID (Fig. 4B) occurs by gradual excitation of the molecule through collisions

193   with a neutral gas. The increasing energy enables conformational and structural

194   rearrangements of the molecule, resulting in higher energy intermediates. The

195   dissociation is initiated by intramolecular proton transfer to the amide oxygen or

196   nitrogen, which destabilizes the amide system. Subsequent cleavage of the weakest bond

197   in the system, namely the amide bond (C–N), leads to the formation of *b* and *y* type

198   fragments, which are a protonated acylium/oxazolone ion and a truncated peptide,

199   respectively. Fig. 4B represents the direct cleavage of the peptide bond, which is typical

200   for high–energy CID[47]. For lower collision energies (as in the case of this study), *b/y* type

201   fragmentation occurs typically through additional rearrangement reactions. Discussion of

202   the possible rearrangement pathways lies beyond the scope of this paper. The reader is

203   referred to an excellent review by Paizs *et al.*[48]
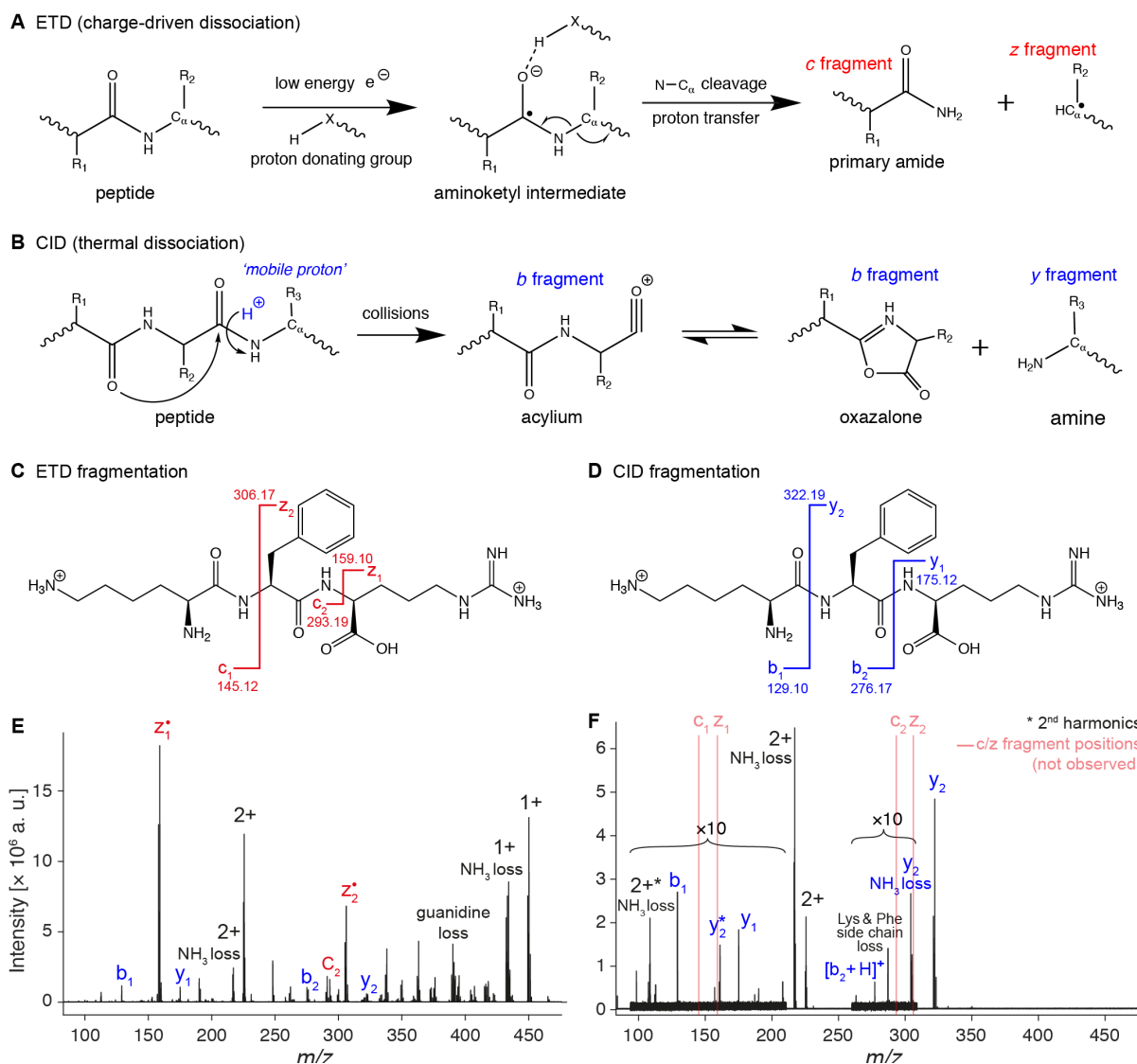
205   **Figure 4.** ETD vs. CID dissociation of peptides. (A) ETD triggers *c/z* type fragmentation, resulting in

206   formation of a primary amide (*c* fragment). (B) CID induces *b/y* type fragmentation, which leads to

207   formation of an acylium ion (*b* ion) that can rearrange to an oxazolone. (C) ETD and (D) CID fragmentation

208   expected for the model tripeptide Lys–Phe–Arg. (E) The ETD spectrum of Lys–Phe–Arg shows intense *c/z*

209   peaks and residual *b/y* signals (present because of the long residence time of the ions in the reaction cell).

210   (F) The CID spectrum of Lys–Phe–Arg shows major *b/y* peaks and no *c/z* fragments. Complete assignment

211   of the mass spectra is presented in Supporting Tables S2 and S3.

In order to directly compare the fragmentation pathways in ETD and TERS, we performed measurements on the same tripeptide Lys–Phe–Arg with both techniques. The sequence was chosen such that: (*i*) there is a basic residue, Arg and Lys, at either end of the peptide to facilitate the formation of a 2+ charge state, (*ii*) the middle amino acid is Phe, which increases the Raman cross section of the molecule. The expected ETD and CID fragmentation pathways of Lys–Phe–Arg are presented in Fig. 4 C and D, respectively. Fig. 4 E and F show the ETD and CID mass spectra of the peptide, acquired in the same experimental setup. In line with the expected fragmentation pathway (Fig. 4C), the ETD spectrum shows strong *c/z* peaks and very weak *b/y* peaks. The residual *b/y* species are most likely formed by collisions within the reaction cell, due to the elevated pressure during electron transfer. Besides *c/z* type fragmentation, we observed significant loss of NH_3 and guanidine from the residues of Arg and Lys, which is also typical for ETD[49]. The CID spectrum of Lys–Phe–Arg (Fig. 4F) shows strong *b/y* peaks and no *c/z* peaks, consistent with the pathway shown in Fig. 4D.

The TER spectra of Lys–Phe–Arg (Fig. 5) indicate the presence of reactions similar to fragmentation in ETD: (*i*) the amide I band is clearly visible at low laser irradiance and disappears gradually upon increase of the laser exposure. This is likely due to *c/z* type fragmentation of the peptide backbone, leading to formation of enolimines (thermodynamically disfavored) or primary amides, which are extremely susceptible to photodamage and decay in TERS even at very low laser irradiance (see examples in Fig. S6 and S7), (*ii*) no ν(C=O) vibrations are observed at 1700 cm^{-1}, which indicates that *b* fragments are not formed – neither acylium, nor oxazolone species (see Fig. 4B), (*iii*) new bands appear at 455 and 1110 cm^{-1}, indicating loss of guanidine from the Arg residue. These bands arise also in the TER spectra of argininamide (Fig. S6). We attribute them to

236 the in–plane C–N scissoring (455 cm⁻¹) and symmetric C–N stretching (1110 cm⁻¹)

237 vibrations of guanidine.

238
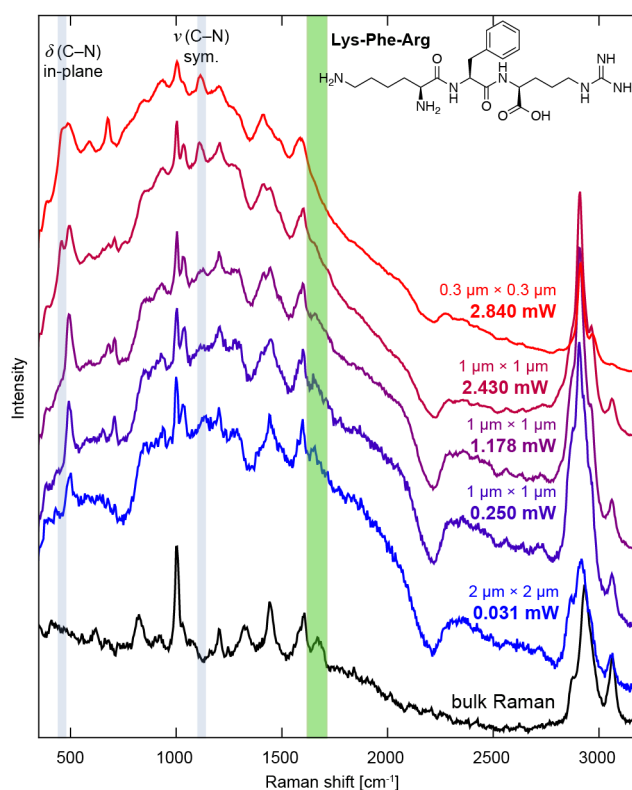
Figure 5. Plasmon–induced dissociation of Lys–Phe–Arg. Similar to the peptides shown in Fig. 3, the TER spectrum acquired at low laser irradiance (blue trace) closely resembles the bulk Raman spectrum of the same compound. Upon increasing the laser irradiance, the amide I band gradually disappears, due to c/z type dissociation of the peptide backbone. We do not observe any peak at 1700 cm⁻¹, which would indicate the formation of b fragments. The new peaks at 455 and 1110 cm⁻¹ likely correspond to loss of guanidine, in line with the ETD spectrum shown in Fig. 4E.

245 The ν(C=O) vibrations of b fragments (oxazolone or acylium–derived carbonyl species)

246 are absent not only in the spectra of Lys–Phe–Arg, but also in the spectra of almost all

247 peptides and proteins under study. The single exception is the TER spectrum of the β–

248 hairpin oligopeptide acquired at 2.840 mW (Fig. 3C). It shows a small side band at

249 1705 cm⁻¹ for maximum laser irradiance and very high temperature under the tip, due to

250 accumulation of heat on a very small acquisition area (0.2–0.3 µm). Hence, in this case,

13

251 thermally driven *b/y* type fragmentation may also occur. Carbonyl vibrations at 1720 cm$^-$

252 ^{1} appear also for the tripeptide Cys–Phe–Phe (Fig. S4). In that case, the 1720 cm^{-1} peak

253 corresponds to the C=O vibration of the carboxyl group on the C–terminus of the peptide,

254 and is observed in both confocal Raman and TER spectra.

255 In order to directly observe the N–C$_\alpha$ dissociation of the amide system, we investigated a

256 small model amide N–methyl–*p*–mercaptobenzamide, whose TER spectrum is simple

257 enough to unambiguously identify the reaction products. Fig. 6B shows a gradual

258 transformation of N–methyl–*p*–mercaptobenzamide into *p*–mercaptobenzamide (Fig. 6A)

259 via plasmon–induced cleavage of the N–C$_\alpha$ bond. Similar to the peptides in Fig. 3 and 5, the

260 TER spectrum acquired at low laser irradiance (blue trace in Fig. 6B) resembles the bulk

261 Raman spectrum of N–methyl–*p*–mercaptobenzamide. The amide I band is very weak in

262 both bulk Raman and TER spectra of this molecule, probably due to the conjugation of the

263 amide system with the benzene ring. Upon increasing the laser power, the amide III band

264 at 1320 cm^{-1} decreases gradually, and arises at 1410 cm^{-1} – the amide III band has a

265 different position for primary and secondary amides. At the same time, a new peak arises

266 at 1195 cm^{-1}, indicating the NH$_2$ rocking vibration of the primary amide. The resulting

267 spectrum looks exactly the same as the TER spectrum of *p*–mercaptobenzamide (blue

268 trace in Fig. 6A), which unambiguously proves *c/z* type fragmentation. A similar

269 experiment was performed for another small amide, N,N–dimethyl–*p*–

270 mercaptobenzamide, and also resulted in preferential scission of the N–C$_\alpha$ bonds (see Fig.

271 S8).

272
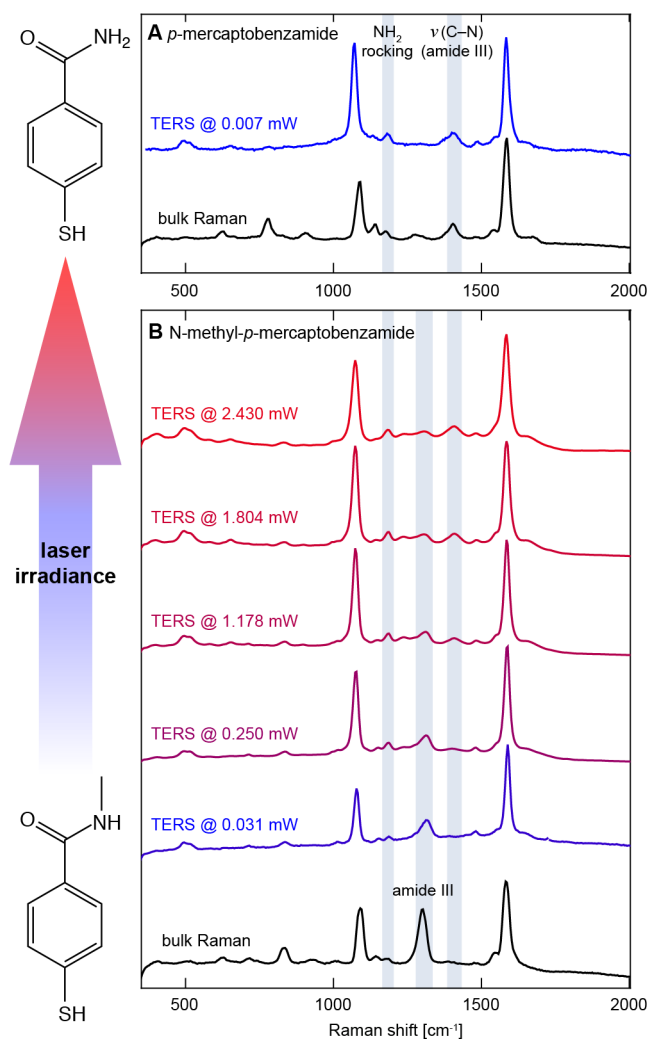
Figure 6. Plasmon–induced N–C$_\alpha$ dissociation of the amide system in N–methyl–p–mercaptobenzamide. Upon increasing the laser irradiance, the secondary amide shown in (B) gradually transforms into a primary amide (A) via c/z type fragmentation of the amide bond.

For both small amides, the observed reaction is clearly driven by electron capture, not by thermal excitation. Similar to peptides, thermal activation would lead to dissociation of the C–N bond (b/y type fragmentation), which is the weakest bond in the molecule. This is illustrated in the CID mass spectra of N–methyl–p–mercaptobenzamide and N,N–dimethyl–p–mercaptobenzamide (Fig. S9), where the dominant fragment is the b ion at m/z = 137.

Discussion

The similarity between the fragments forming in TERS and ETD supports the idea of an electron–capture–induced and radical–mediated process, brought forward in our recent work[5]. Furthermore, it might also indicate a similarity of the reaction pathways in ETD and TERS, although we do note that the molecules in ETD are charged, which may affect the energetics of the electron capture and fragmentation process. However, considering the proposed pathway in ETD (Figure 4A), the electron could analogously reside in the π^* orbital of the C=O group, while the protonation might be an intra– or intermolecular process involving acidic functional groups, instead of the protonated base.

The $N-C_\alpha$ dissociation of the peptide backbone is not the only reaction observed in the reported TERS experiments, likely for two reasons. Firstly, the homolytic c/z fragmentation results in the formation of radical $z^\bullet$ species, which may undergo further charge–driven reactions[43]. Secondly, similar to ETD, the hot carriers may trigger the loss of amino acid side chains and reactions therein[49,50]. For example, the capture of a hot electron by the benzyl group leads to a benzyl–centered radical that binds to the aromatic systems of neighboring molecules. This reaction, previously reported for benzyl mercaptan[5], leads to a decrease in the intensity of the ring breathing modes at 1000 cm^{-1} and to a broadening of the ring stretching bands at 1600 cm^{-1}, as observed in Figures 1B, 3B&C and 5.

At the same time, the presented data does not allow the estimation of the reaction yield. In particular, the backbone fragmentation may involve less than 100% of the peptide bonds present in the sample, leading to a residual intensity of the amide I band in the TER spectra, or to the presence of a side shoulder (see Figures S2–S5). Accordingly, we do not

16

305 claim that the amide I band disappears completely from the spectra of all the peptides

306 measured. Instead, we notice that the TER spectra acquired at non–destructive, mild

307 conditions (blue traces in Figs. 3, 5, S2–S5) include a well–resolved amide I peak, similar

308 to the bulk Raman spectra of the same peptides (black traces), and contrary to the spectra

309 acquired at high laser irradiance (red traces). The lack of a well–resolved amide I band in

310 the TER spectra of proteins and peptides is a landmark of photoinduced sample

311 degradation. Such spectra may no longer reflect the native structure of the protein and

312 should not be interpreted, nevertheless they are frequently presented in the TERS

313 literature (see Table S1).

314 The spectral changes described in this paper are clearly a result of charge–driven

315 reactions and cannot be explained by a thermal mechanism. In particular, thermal

316 broadening of the TER spectral lines, which could possibly lead to merging of neighboring

317 peaks, is very small (3–5 cm^{-1}) for the temperature range investigated in this study. See

318 Section S6 for a detailed dicussion.

319 The presented analogy between gas–phase reactions and ambient TERS has its

320 limitations. ETD and CID MS are carried out in vacuum, whereas TERS is typically

321 conducted in ambient conditions, with high availability of water and oxygen at the

322 reaction site. Hence, the reactive species forming upon the dissociation may lead to

323 different final products in MS and TERS experiments. For example, the acylium b ion

324 formed in CID of peptides, tautomerizes to an oxazolone structure in the gas phase (Fig.

325 4B)[51,52], whereas at ambient conditions a truncated amino acid could be formed by the

326 addition of water. Oxygen and traces of water are generally present in ambient conditions

327 and may thus play a role in TERS. An extreme example is the disappearance of the amide

328 I band in the SER spectra of BSA upon treatment with H_2O_2, observed by Xu *et al.* [40]. In

329   that case, the HO• radical likely abstracts hydrogen from the α–carbon site, which

330   eventually results in the formation of either an α–ketoamide or imide[53] by subsequent

331   reactions with oxygen and water. Despite the fact that oxygen and hydroxyl radicals may

332   be formed during the TERS process, we did not observe any of evidence for the expected

333   products in the present study. This renders a HO•–mediated degradation pathway

334   unlikely to be the dominant reason for the disappearance of the amide I band in ambient

335   TERS.

336 **Conclusions**

337   We demonstrated that plasmon–induced hot electrons can dissociate peptides, and

338   postulate that the underlying chemistry is analogous to the one known from the gas–

339   phase studies of low energy electron attachment. Our findings are consistent for a

340   comprehensive selection of model systems (10 molecules of various sizes). The identity

341   of fragments produced in ETD and plasmon–driven photocatalysis suggests that

342   intuitions from the gas–phase electron capture can be transferred at least partially to

343   plasmon–assisted catalysis on noble metal nanoparticles. Literature on dissociative

344   electron capture in the gas phase covers a broad scope of reactants, including

345   biomolecules – beyond small molecules and model thiols used in plasmon–assisted

346   catalysis. We postulate that the nonergodic chemical transformations known from the

347   electron attachment literature may be triggered by plasmonic nanostructures. These

348   pathways can be activated only by hot carriers (not by phonons), hence they are

349   considered 'impossible' within the framework of conventional (thermally activated)

350   catalysis. Performing these reactions at ambient pressure and room temperature would

351   be a valuable addition to the toolbox of chemical synthesis.

352 At the same time, these results resolve a long–lasting controversy in plasmonically

353 enhanced Raman experiments of peptides and proteins. We show that the disappearance

354 of the amide I band is caused by excessive energy deposition on the sample and is a sign

355 of peptide backbone degradation. Mild excitation (low laser power and short irradiation)

356 permits the acquisition of reliable TER spectra containing the amide I band.

357 To conclude, we postulate that TER spectra that include unexpected peaks and have little

358 in common with the corresponding Raman spectra should be critically appraised. Such

359 spectral changes are probably caused by some interesting chemistry occurring under the

360 TERS tip, which can now be predicted using the theoretical framework of DIET and ETD.

361 At the same time, we demonstrate that the reproducibility of TER spectra can be

362 dramatically improved by using mild measurement conditions (see Fig. S10), making

363 TERS a more reliable and reproducible analytical technique.

364 **Methods**

365 **TERS measurements.** TERS measurements were conducted similar to the previous work

366 by our group[5,54,55]. Briefly, we performed top–illumination TERS with Ag tips and Au

367 substrates (gap mode). We used a scanning tunneling microscope (STM; Ntegra Spectra

368 Upright, NT–MDT), equipped with a 0.7 NA 100× objective (Mitutoyo), coupled to a

369 Raman spectrometer (Solar T–II, NT–MDT) with a CCD (Newton 971 UVB, Andor)

370 thermoelectrically cooled to –85 °C.

371 The STM was operated in constant current mode. In principle, the tunneling electrons

372 could induce similar reactions as the plasmon-induced hot carriers, similar as in inelastic

373 electron tunneling spectroscopy[10,56]. However, such reactions can occur only if the

374 energy of the tunneling electron (*i. e.* the bias voltage) matches the energy of the

375   unoccupied orbitals of the molecular adsorbates. For organic molecules, this energy

376   typically exceeds 0.5 V. Therefore, we used a low bias voltage (0.1 V applied to the sample)

377   to avoid injection of tunneling electrons into the investigated molecules.

378   TERS tips were obtained by electrochemical etching, according to the procedure

379   described in ref. [57]. TER spectra were acquired on square grids with 100–400 pixels

380   (from 10×10 to 20×20 pixels), with laser illumination at 632.8 nm (HeNe laser) and

381   laser power between 0.007 and 2.880 mW. The integration time was 1–3 s. The TER

382   spectra presented in Fig. 1, 3, 5, 6, S2–S8 and S10–S11 are average spectra accumulated

383   over grids of pixels.

384   **Confocal Raman measurements.** Confocal Raman spectra of bulk samples were

385   obtained using the same instrument as TER spectra. The laser power was 2.88 mW and

386   the integration time was 60 s.

387   **Substrates.** Template–stripped Au substrates were prepared according to the protocol in

388   ref. [58,59]. Briefly, a Si wafer (SSP, Siegert Wafer) was pre-cleaned by soaking in a piranha

389   solution ($H_2SO_4 : H_2O_2$ 30%, 7 : 3 v/v) for 30 minutes, rinsed with Milli–Q water and dried

390   under a N_2 stream. Next, 150 nm of Au (99.99%, Acros) were thermally evaporated

391   (BAL–TEC MCS 010) on the clean Si wafer at a deposition rate of 0.05–0.10 nm/s, under

392   a pressure of 1×10^{-6} mbar. Glass substrates (25 mm x 7 mm x 1 mm) were attached onto

393   the Au layer using the Norland Optical Adhesive No. 61. The glue was cured by 20 minutes

394   of UV irradiation and overnight heating to 50 °C. The glass substrates were stripped off

395   the Si wafer directly before the sample preparation, revealing a flat and clean Au surface

396   on the glass support.

397   **Samples.** Thin layers of peptides were formed on the Au surface using three methods:

- self–assembly for all molecules including –SH groups (overnight incubation of the substrate in a solution of the amide/peptide/protein; 1 mM ethanolic solution for N–methyl–*p*–mercaptobenzamide, N,N–dimethyl–*p*–mercaptobenzamide and *p*–mercaptobenzamide, Cys–Phe, Cys–Phe–Phe; 100 µg/mL aqueous solution for the α–helical and β–hairpin peptides, and for the Cys–terminated BSA),

- dried–droplet deposition for molecules without –SH groups (40 µL of 1 mM solution in water, dried in a desiccator at 15 mbar for Arg–Phe and Phe–Phe) – the TERS measurements were conducted in the center of the dried–droplet ring, where the sample was evenly distributed at a low coverage,

- spin coating for Lys–Phe–Arg, because it formed large crystals upon dried droplet deposition (40 µL of 1 mM of solution was casted on the substrate spinning at 750 rpm for 1 min).

N–methyl–*p*–mercaptobenzamide, N,N–dimethyl–*p*–mercaptobenzamide and *p*–mercaptobenzamide were purchased from Chemspace (Riga, Latvia; synthesis by FCH Group, Kiev, Ukraine). Arg–Phe (> 99%) was obtained from Bachem. Phe–Phe (≥ 98%) and L–argininamide dihydrochloride (≥ 98%) were purchased from Aldrich. Cys–Phe (≥ 98%) and Cys–Phe–Phe (≥ 98%) were acquired from CanPeptide (Montréal, Canada). 3–phenylpropionamide (97%) was obtained from ABCR. Lys–Phe–Arg (97.6%), α–helical (94.5%) and β–hairpin (92.6%) peptides were purchased from GenScript (Piscataway, NJ). Cys–modified BSA (> 98%) was obtained from ProteinMods (Madison, WI).

ETD and CID measurements. ETD and CID experiments were performed on a Bruker solariX (Bruker Daltonics GmbH, Bremen, Germany) Fourier–transform ion cyclotron resonance mass spectrometer. Molecular ions of the tripeptide Lys–Phe–Arg were generated by electrospray ionization, and the doubly protonated species (m/z=225.64)

422 was isolated. ETD experiments were carried out using methane radical anions as transfer

423 reagent and reaction times of 400 ms. Radical anions were generated by chemical

424 ionization within the instrument. Additionally, CID experiments were conducted on the

425 doubly charged peptide ion for comparison. Collision energies of 3.0 eV were employed.

426 Complete peak assignments of the ETD and CID spectra of Lys–Phe–Arg are presented in

427 Tables S2 and S3. We note that the sample obtained was contaminated with a C–

428 terminally amidated derivative of the tripeptide (Lys–Phe–Arg–NH$_2$). Thanks to the

429 excellent mass resolution of the FTICR analyser, we could discriminate between the amide

430 (M$_2$) and the free acid (M$_1$) and assign the peaks for both forms. The fragment ions *c* and

431 *y* always lose an additional hydrogen atom during fragmentation (see mechanism above),

432 which is included in the peak assignment without further comment.

433 **3D peptide structures.** The 3D structures of the α–helical and β–hairpin peptides shown

434 in Fig. 2 were obtained using PEP–FOLD3 software[60], freely accessible online at

435 http://bioserv.rpbs.univ-paris-diderot.fr/services/PEP-FOLD3/ .

Supporting Information

437 Supporting information available: summary of the presence/absence of the amide I band

438 in the TERS literature, effect of the size if the TERS image on the hot spot temperature,

439 comparison of the position of the amide I band in bulk Raman and TER spectra, TERS

440 measurements of Phe–Phe, Cys–Phe, Cys–Phe–Phe, the α–helical peptide, N,N–dimethyl–

441 *p*–mercaptobenzamide, argininamide and 3–phenylpropionamide, CID MS of N–methyl–

442 *p*–mercaptobenzamide and N,N–dimethyl–*p*–mercaptobenzamide, peak assignment of

443 the ETD and CID spectra of Lys–Phe–Arg, TER spectra of Arg–Phe acquired with five

444 different tips, quantification of thermal broadening of TER spectral lines.

Acknowledgements

Author Contributions

J. S. conceived the project, performed the TERS experiments and wrote the first manuscript. J. B. M. designed the MS experiments and interpreted their results. All authors interpreted the TERS results, selected the model compunds and corrected the manuscript.

Data Availability

The data used in this publication are freely accessible from a curated data archive at ETH Zurich (https://www.research-collection.ethz.ch) under the DOI ...

Note

The authors declare no competing financial interest.

Literature

[1]   D. B. Ingram, S. Linic, *J. Am. Chem. Soc.* **2011**, *133*, 5202.

[2]   P. Christopher, H. Xin, S. Linic, *Nat. Chem.* **2011**, *3*, 467.

[3]   L. Zhou, D. F. Swearer, C. Zhang, H. Robatjazi, H. Zhao, L. Henderson, L. Dong, P. Christopher, E. A. Carter, P. Nordlander, N. J. Halas, *Science (80-.).* **2018**, *362*, 69.

[4]   E. M. van Schrojenstein Lantman, T. Deckert-Gaudig, A. J. G. Mank, V. Deckert, B. M.

Weckhuysen, *Nat. Nanotechnol.* **2012**, *7*, 583.

[5] J. Szczerbiński, L. Gyr, J. Kaeslin, R. Zenobi, *Nano Lett.* **2018**, *18*, 6740.

[6] S. Mukherjee, F. Libisch, N. Large, O. Neumann, L. V. Brown, J. Cheng, J. B. Lassiter, E. A. Carter, P. Nordlander, N. J. Halas, *Nano Lett.* **2013**, *13*, 240.

[7] B. De Nijs, F. Benz, S. J. Barrow, D. O. Sigle, R. Chikkaraddy, A. Palma, C. Carnegie, M. Kamp, R. Sundararaman, P. Narang, O. A. Scherman, J. J. Baumberg, *Nat. Commun.* **2017**, *8*, 1.

[8] T. E. Tesema, B. Kafle, M. G. Tadesse, T. G. Habteyes, *J. Phys. Chem. C* **2017**, *121*, 7421.

[9] J.-H. Zhong, X. Jin, L. Meng, X. Wang, H.-S. Su, Z.-L. Yang, C. T. Williams, B. Ren, *Nat. Nanotechnol.* **2016**, *12*, 132.

[10] E. Kazuma, J. Jung, H. Ueba, M. Trenary, Y. Kim, *Science (80-.).* **2018**, *360*, 521.

[11] S. Linic, U. Aslam, C. Boerigter, M. Morabito, *Nat. Mater.* **2015**, *14*, 567.

[12] P. Avouris, R. E. Walkup, *Annu. Rev. Phys. Chem.* **1989**, *40*, 173.

[13] G. Ertl, in *Handb. Heterog. Catal.*, Wiley-VCH, Weinheim, Germany, **2008**, pp. 1462–1479.

[14] W. Ho, *J. Phys. Chem.* **1996**, *100*, 13050.

[15] T. E. Madey, *Science* **1986**, *234*, 316.

[16] M. Bonn, S. Funk, C. Hess, D. N. Denzler, C. Stampfl, M. Scheffler, M. Wolf, G. Ertl, *Science (80-.).* **1999**, *285*, 1042.

[17] C. Frischorn, M. Wolf, *Chem. Rev.* **2006**, *106*, 4207.

[18] P. E. Laibinis, R. L. Graham, H. A. Biebuyck, G. M. Whitesides, *Science (80-.).* **1991**, *254*, 981.

[19] J. S. Suh, N. H. Jang, D. H. Jeong, M. Moskovits, *J. Phys. Chem.* **1996**, *100*, 805.

[20] D. Kurouski, R. P. Van Duyne, I. K. Lednev, *Analyst* **2015**, *140*, 4967.

[21] T. Schmid, L. Opilik, C. Blum, R. Zenobi, *Angew. Chem. Int. Ed. Engl.* **2013**, *52*, 5940.

[22] A. Otto, *J. Raman Spectrosc.* **2002**, *33*, 593.

[23] K. F. Domke, D. Zhang, B. Pettinger, *J. Phys. Chem. C* **2007**, *111*, 8611.

[24] P. C. Andersen, M. L. Jacobson, K. L. Rowlen, *J. Phys. Chem. B* **2004**, *108*, 2148.

[25] E. J. Bjerneld, P. Johansson, M. Käll, *Single Mol.* **2000**, *1*, 239.

496 [26] R. Böhme, M. Richter, D. Cialla, P. Rösch, V. Deckert, J. Popp, *J. Raman Spectrosc.*
497   **2009**, *40*, 1452.

498 [27] A. Nakata, T. Nomoto, T. Toyota, M. Fujinami, *Anal. Sci.* **2013**, *29*, 865.

499 [28] S. Bonhommeau, D. Talaga, J. Hunel, C. Cullin, S. Lecomte, *Angew. Chemie - Int. Ed.*
500   **2017**, *56*, 1771.

501 [29] L. Li, T. Hutter, U. Steiner, S. Mahajan, *Analyst* **2013**, *138*, 4574.

502 [30] F. Pashaee, M. Tabatabaei, F. A. Caetano, S. S. G. Ferguson, F. Lagugné-Labarthet,
503   *Analyst* **2016**, *141*, 3251.

504 [31] T. Deckert-Gaudig, V. Deckert, *Curr. Opin. Chem. Biol.* **2011**, *15*, 719.

505 [32] L. E. Hennemann, A. J. Meixner, D. Zhang, *Spectroscopy* **2010**, *24*, 119.

506 [33] Z. He, Z. Han, M. Kizer, R. J. Linhardt, X. Wang, A. M. Sinyukov, J. Wang, V. Deckert,
507   A. V. Sokolov, J. Hu, M. O. Scully, *J. Am. Chem. Soc.* **2019**, *141*, 753.

508 [34] C. Blum, T. Schmid, L. Opilik, N. Metanis, S. Weidmann, R. Zenobi, *J. Phys. Chem. C*
509   **2012**, *116*, 23061.

510 [35] D. Kurouski, T. Postiglione, T. Deckert-Gaudig, V. Deckert, I. K. Lednev, *Analyst*
511   **2013**, *138*, 1665.

512 [36] G. D. Chumanov, R. G. Efremov, I. R. Nabiev, *J. Raman Spectrosc.* **1990**, *21*, 43.

513 [37] M. De Li, Y. Cui, M. X. Gao, J. Luo, B. Ren, Z. Q. Tian, *Anal. Chem.* **2008**, *80*, 5118.

514 [38] J. Y. Huang, C. Zong, L. J. Xu, Y. Cui, B. Ren, *Chem. Commun.* **2011**, *47*, 5738.

515 [39] M. Feng, H. Tachikawa, *J. Am. Chem. Soc.* **2008**, *130*, 7443.

516 [40] L. J. Xu, C. Zong, X. S. Zheng, P. Hu, J. M. Feng, B. Ren, *Anal. Chem.* **2014**, *86*, 2238.

517 [41] P. Matteini, M. Cottat, F. Tavanti, E. Panfilova, M. Scuderi, G. Nicotra, M. C.
518   Menziani, N. Khlebtsov, M. De Angelis, R. Pini, *ACS Nano* **2017**, *11*, 918.

519 [42] X. M. Lin, Y. Cui, Y. H. Xu, B. Ren, Z. Q. Tian, *Anal. Bioanal. Chem.* **2009**, *394*, 1729.

520 [43] N. Leymarie, C. E. Costello, P. B. O'Connor, *J. Am. Chem. Soc.* **2003**, *125*, 8949.

521 [44] L. Elviri, in *Tandem Mass Spectrom. - Appl. Princ.*, IntechOpen, London, **2012**, pp.
522   161–178.

523 [45] L. Sleno, D. A. Volmer, *J. Mass Spectrom.* **2004**, *39*, 1091.

524 [46] F. Tureček, R. R. Julian, *Chem. Rev.* **2013**, *113*, 6691.

525 [47] J. E. P. Syka, J. J. Coon, M. J. Schroeder, J. Shabanowitz, D. F. Hunt, *Proc. Natl. Acad.*
526   *Sci.* **2004**, *101*, 9528.

527   [48]   B. Paizs, S. Suhal, *Mass Spectrom. Rev.* **2005**, *24*, 508.

528   [49]   Q. Xia, M. V. Lee, C. M. Rose, A. J. Marsh, S. L. Hubler, C. D. Wenger, J. J. Coon, *J. Am.*
529   *Soc. Mass Spectrom.* **2011**, *22*, 255.

530   [50]   Y. M. E. Fung, T. W. D. Chan, *J. Am. Soc. Mass Spectrom.* **2005**, *16*, 1523.

531   [51]   A. G. Harrison, *Mass Spectrom. Rev.* **2009**, *28*, 640.

532   [52]   J. Grzetic, J. Oomens, *J. Am. Soc. Mass Spectrom.* **2012**, *23*, 290.

533   [53]   G. Xu, M. R. Chance, *Chem. Rev.* **2007**, *107*, 3514.

534   [54]   M. Paulite, C. Blum, T. Schmid, L. Opilik, K. Eyer, G. C. Walker, R. Zenobi, *ACS Nano*
535   **2013**, *7*, 911.

536   [55]   L. Opilik, P. Payamyar, J. Szczerbiński, A. P. Schütz, M. Servalli, T. Hungerland, A. D.
537   Schlüter, R. Zenobi, *ACS Nano* **2015**, *9*, 4252.

538   [56]   W. Ho, *J. Phys. Chem.* **1996**, *100*, 13050.

539   [57]   W. Zhang, B. S. Yeo, T. Schmid, R. Zenobi, *J. Phys. Chem. C* **2007**, *111*, 1733.

540   [58]   E. A. Weiss, G. K. Kaufman, J. K. Kriebel, Z. Li, R. Schalek, G. M. Whitesides,
541   *Langmuir* **2007**, *23*, 9686.

542   [59]   J. Stadler, T. Schmid, L. Opilik, P. Kuhn, P. S. Dittrich, R. Zenobi, *Beilstein J.*
543   *Nanotechnol.* **2011**, *2*, 509.

544   [60]   A. Lamiable, P. Thévenet, J. Rey, M. Vavrusa, P. Derreumaux, P. Tufféry, *Nucleic*
545   *Acids Res.* **2016**, *44*, W449.

546